Catalysis Science & Technology

ROYAL SOCIETY OF CHEMISTRY

PAPER

View Article Online
View Journal | View Issue

Cite this: *Catal. Sci. Technol.*, 2025, 15, 4024

Minimizing radiative and nonradiative energy leakage in red-light-absorbing supramolecular nanoassemblies to boost oxidative photocatalytic activity in water†

Aditya Singh, Manoj Kumar and Vandana Bhalla *

Harnessing abundant red-light, which constitutes a significant portion of solar radiation, to energize oxidative transformations is an economic and eco-friendly strategy for sustainable chemistry. Given this consideration, red-light-absorbing J-type nanoassemblies based on a donor–acceptor–donor (D–A–D) building block (**BrTPA-Py**) with 4-bromo-*N*,*N*-diphenylaniline as the donor and pyrazino[2,3-b]pyrazine-2,3-dicarbonitrile as the acceptor have been developed in aqueous media. The strategic incorporation of bromine atoms at the periphery enhanced spin–orbit coupling and restricted nonradiative/radiative decay through bromine···bromine noncovalent interactions. Due to the synergistic effect of strong charge-transfer characteristics, presence of bromine atoms and restricted inter/intramolecular motion, rapid intersystem crossing (ISC) is facilitated in **BrTPA-Py** nanoassemblies, enabling the activation of aerial oxygen through type I (electron transfer) and/or type II (energy transfer) pathways upon irradiation by red-light. The remarkable photosensitization potential of **BrTPA-Py** nanoassemblies has been unveiled to catalyse the oxidation of phosphines and hydroxylation of arylboronic acids under red-light irradiation, which is unprecedented. This investigation presents a simple design strategy to propel advances in sustainable photocatalysis by regulating the dynamics of excited state under low-energy radiation through the incorporation of halogen atoms in the backbone of the building block with strong charge-transfer characteristics.

Received 4th February 2025,
Accepted 27th May 2025

DOI: 10.1039/d5cy00131e

rsc.li/catalysis

Introduction

Recently, the development of easy to prepare, economic, photocatalytic systems that work under low-energy red-light radiation to catalyse organic transformations under eco-friendly conditions has attracted significant research attention. Unlike reactions powered by high-energy radiation, low-energy red-light-mediated reactions generate minimal side products, as a result of which the reaction efficiency is increased with wide substrate scope and enhanced functional group permissiveness.[1] This field is growing, and more recently, the catalytic potential of red-light-absorbing natural photosensitizers (chlorophyll) and synthetic photosensitizers (covalent organic frameworks/conjugated microporous polymers/porous organic polymers) has been demonstrated for photocatalytic systems in oxidative organic transformations.[2–6] Though unprecedented, the preparation/separation (of natural products) of these photosensitizers is still difficult, and to enrich the knowledge framework for the subsequent design of photocatalysts with strong absorption in the low-energy region, a thorough analysis of the structure–activity relationship is essential. Red-light-absorbing organic 'metal-free' photosensitizers stand out as potential catalysts due to their designability, synthetic convenience, cost-effectiveness, tunable optical properties, and low toxicity. Furthermore, the potential of organic photosensitizers to activate aerial oxygen through electron transfer (type I) and/or energy transfer (type II) pathways for the generation of reactive oxygen species (ROS) as strong oxidants under reaction conditions provide additional opportunities to catalyse oxidative organic transformations under 'additive-free' conditions.[7,8] Currently, extensive efforts have been focused on understanding the design rules to be translated into boosting sensitizing activity by tuning the excited state without paying much attention to ground-state properties. Accordingly, plenty of information is available to regulate the excited state using high-energy radiation as a source of energy (such as blue/green/white light), but there is limited information available to control the dynamics of the excited state under low-energy radiation. Recently, significant research efforts have been focused on the development of red-light-absorbing photosensitizers with

Department of Chemistry, UGC Sponsored Centre of Advance Studies-II, Guru Nanak Dev University, Amritsar-143005, Punjab, India.
E-mail: vanmanan@yahoo.co.in

† Electronic supplementary information (ESI) available. See DOI: https://doi.org/10.1039/d5cy00131e

potential applications in photodynamic therapy (PDT) and photothermal therapy (PTT),[9,10] but research efforts to prepare photocatalytic photosensitizers are still in their infancy. Despite great similarities in their working mechanism, while designing photocatalytic photosensitizers, various other factors such as the photostability of the catalyst, and its interactions with nucleophile/oxygen need urgent attention, and hence, their structural features ought to differ.

Our research work involves the development of photocatalytic photosensitizing nanoassemblies for carrying out oxidative organic transformations under sustainable reaction conditions.[11–14] Compared to photocatalysts based on small organic molecules, photocatalytic supramolecular nanoassemblies are advantageous due to their high photostability and amplified photosensitization activity. Recently, we reported the development of twisted intramolecular charge transfer (TICT)-active photosensitizing nanoassemblies based on the D–A–D system (**TPA-Br**) with bromine atoms at the periphery (Fig. 1a).[15]

Due to the combined effect of charge-transfer characteristics, and the incorporation of bromine (enhanced spin–orbit coupling (SOC) and halogen···halogen noncovalent interactions) in **TPA-Br** nanoassemblies, nonradiative decay was significantly suppressed and radiative decay (through phosphorescence) was blocked, promoting intersystem crossing (ISC)/reverse intersystem crossing (RISC) between triplet excited state and singlet excited state energy levels. Thereupon, **TPA-Br** nanoassemblies exhibited remarkable type I and type II photosensitization activity in aqueous media. Nonetheless, **TPA-Br** nanoassemblies absorbed in the blue region of visible-light irradiation and exhibited radiative leakage through fluorescence. From this perspective, we planned to optimise the structure of the building block to produce red-light-absorbing photosensitizing nanoassemblies with completely restricted radiative (fluorescence and phosphorescence) and nonradiative decay. In view of the successful suppression of nonradiative decay and partial restriction of radiative decay in the compound **TPA-Br**, we planned to retain the design concept built around triphenylamine donors equipped with bromine atoms at the periphery (Fig. 1a). Since strong donor–strong acceptor systems are known to exhibit absorption in the red-light region with restricted fluorescence, we planned to enhance the charge-transfer characteristics of the building block by incorporating a strong acceptor. With information from the literature and our

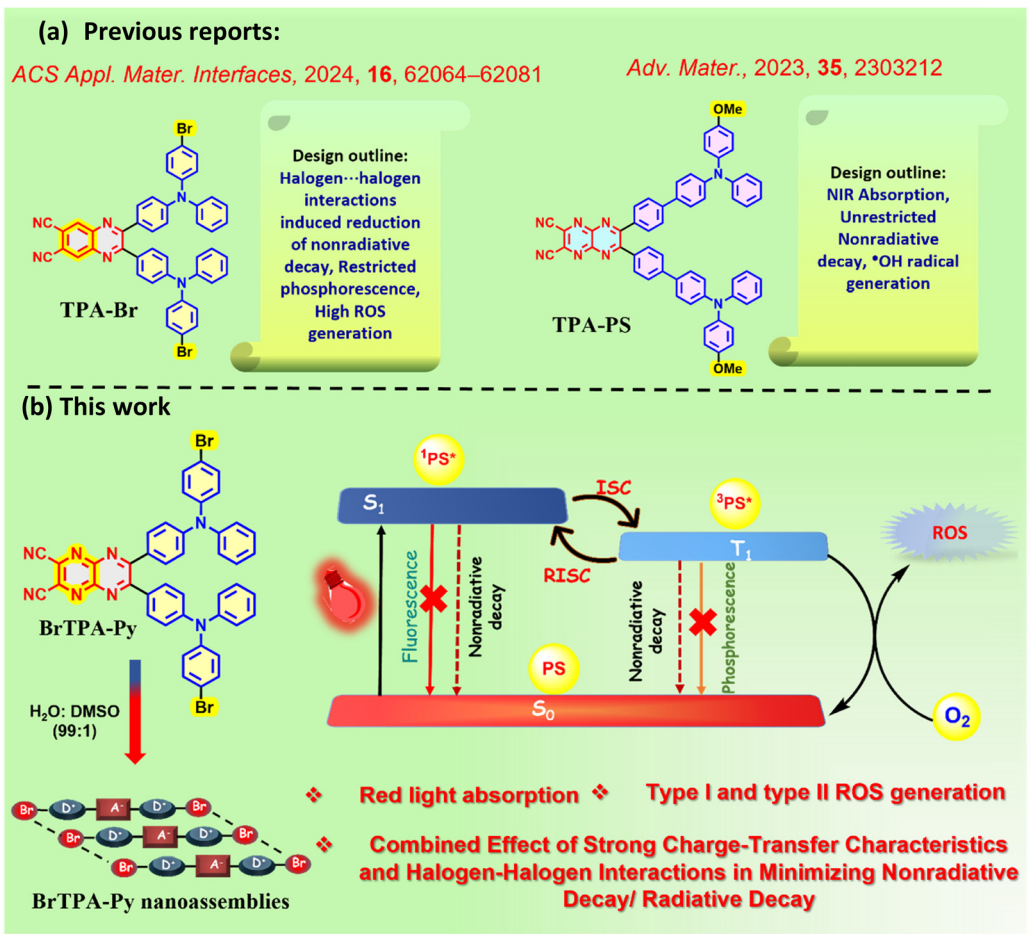

Fig. 1 (a) Previous studies on strong D–A–D systems. (b) Proposed design strategy for the generation of red-light-absorbing **BrTPA-Py** nanoassemblies.

experience from the field, we designed the synthesis of building block **BrTPA-Py** with pyrazino[2,3-*b*]pyrazine-2,3-dicarbonitrile as the strong acceptor and 4-bromo-*N*,*N*-diphenylaniline as the donor (Fig. 1b). We envisaged that, due to strong charge-transfer characteristics, rotatable phenyl groups, and the presence of bromine-atom-induced halogen···halogen interactions, D–A–D building block **BrTPA-Py** will undergo self-assembly to generate J-aggregates with strong absorption in the red-light region with restricted radiative/nonradiative decay in mixed aqueous media. Interestingly, preliminary analysis of electrochemical studies of as-prepared **BrTPA-Py** points to the existence of relatively more stabilised highest occupied molecular orbital (HOMO) and lowest unoccupied molecular orbital (LUMO) energy levels with a reduced band gap compared to compound **TPA-Br**, which supports the relatively strong charge-transfer characteristics of the designed molecule. Absorption studies of **BrTPA-Py** in mixed aqueous media also supported its potential to undergo self-assembly in aqueous media. Although the building block **BrTPA-Py** showed structural similarity to the already-reported compound **TPA-PS** with methoxy (–OMe) groups at its periphery (Fig. 1a), it exhibited distinct photosensitizing properties in the assembled state. The presence of methoxy (–OMe) groups created a spatial separation between **TPA-PS** molecules even in the aggregate state; hence, rotation of the phenyl groups was not completely restricted.[16] As a result, the **TPA-PS** nanoassemblies demonstrated conversion of absorbed energy to thermal energy and generated ·OH radicals through photoinduced electron transfer to oxygen *via* collisions, followed by favourable protonation and subsequent disproportionation reactions. In contrast, compound **BrTPA-Py** generated J-aggregates in mixed aqueous media and all the intramolecular motions were completely hampered. This is attributed to the combined effect of a poor co-solvent (water) and bromine···bromine noncovalent interactions. Consequently, **BrTPA-Py** nanoassemblies exhibited an exceptional ability to activate molecular oxygen through energy transfer as well as electron transfer pathways to generate singlet oxygen and superoxide radical anions in an H_2O : DMSO (99 : 1) solvent mixture under red-light irradiation. Further, the analogue of **BrTPA-Py** without a bromine atom has already been reported to exhibit insignificant activation of aerial oxygen, strongly emphasizing the important contribution of halogen···halogen interactions to ROS generation.[17] These studies highlight the influence of subtle modifications of the structural component of the building block over the photosensitizing activity of the assemblies. While we were compiling this work, the development of near-infrared (NIR)-absorbing π-conjugated polymeric system/semiconducting polymers was reported, in which radiative decay blockage was achieved,[18,19] through the incorporation of heavy atoms in the backbone of the photosensitizers.[18–20] However, besides tedious synthesis, low photostability and insolubility in most solvents, these polymeric materials suffer from low singlet oxygen quantum yields due to unrestricted nonradiative decay. In contrast, the building block **BrTPA-Py** is easy to prepare, freely soluble in common organic solvents and undergoes spontaneous self-assembly by regulating a portion of the co-solvent to generate photostable red-light-absorbing supramolecular nanoassemblies. Due to their well-regulated photosensitization potential, **BrTPA-Py** nanoassemblies in a photoactive state catalysed the oxidation of phosphines (*via* the type II pathway) and the oxidative hydroxylation of arylboronic acids (*via* the type I pathway in the presence of a sacrificial donor) in aqueous media upon irradiation with red-light, which is unprecedented. In contrast to previously developed catalytic systems for these reactions, which have several drawbacks, such as tedious preparation, the requirement for organic media, high catalyst loading, and reliance on blue-LED irradiation as the energy source for efficient functioning, our photocatalyst is easy to prepare, requires minimal catalyst loading, and exhibits controllable and efficient type I and type II ROS generation in water, and thus efficiently catalyses a range of oxidative transformations under low-energy radiation in water (Tables S1 and S2, ESI†). The approach being reported in this paper relies on strong charge-transfer characteristics, the presence of bromine atoms and restricted inter/intra molecular motion of the **BrTPA-Py** nanoassemblies, endowing them with remarkable type I/type II photosensitizing activity in water under red-LED irradiation and offering an economical and eco-friendly strategy toward sustainable chemistry.

Results and discussion

The target D–A–D compound, 6,7-bis(4-((4-bromophenyl)(phenyl)amino)phenyl)pyrazino[2,3-*b*]pyrazine-2,3-dicarbonitrile (**BrTPA-Py**), was synthesized in 58% yield by a condensation reaction between 1,2-bis(4-((4-bromophenyl)(phenyl)amino)phenyl)ethane-1,2-dione (**1**) and 5,6-diaminopyrazine-2,3-dicarbonitrile (**2**) under standard reaction conditions (Scheme 1). The synthesized compound **BrTPA-Py** was fully characterized using various spectroscopic techniques, such as ^{1}H NMR, ^{13}C NMR and HRMS.

After complete characterization of **BrTPA-Py**, we examined its solvent-dependent photophysical behaviour using UV-vis and fluorescence spectroscopic techniques (Fig. 2). A toluene solution of compound **BrTPA-Py** exhibits sharp absorption bands at 300 nm and 376 nm and a broad band at 584 nm (Fig. 2a). Upon gradually increasing the polarity of the solvent (THF/DMSO/EtOH), the absorption pattern remains the same but a blue-shift in the absorption band at longer wavelength ($\Delta\lambda_{abs}$ = 14, 19 nm) is observed, supporting the negative solvatochromism of **BrTPA-Py**.[21] This is ascribed to the

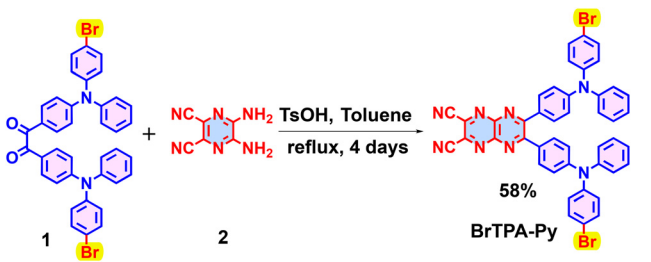

Scheme 1 Synthesis of compound **BrTPA-Py**.

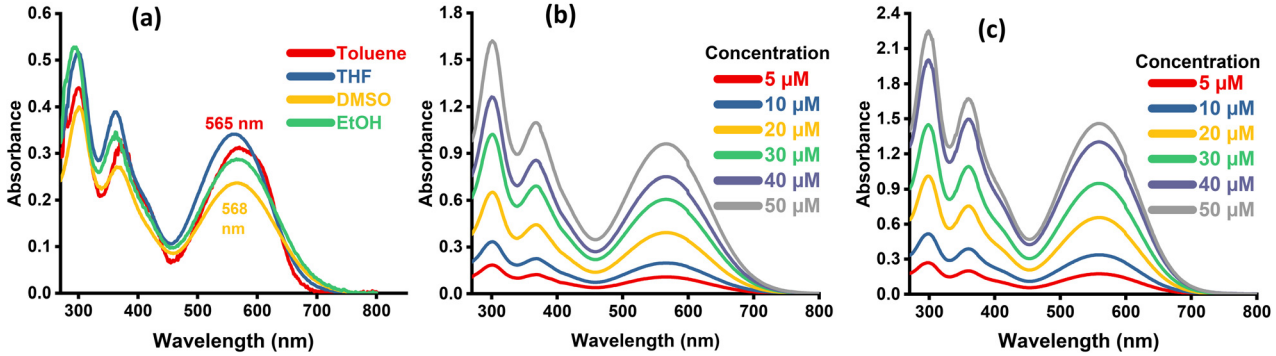

Fig. 2 (a) The UV-vis spectra of **BrTPA-Py** (10 μM) in different solvents. Concentration-dependent UV-vis spectra of **BrTPA-Py** (5–50 μM) in (b) DMSO and (c) THF.

generation of a highly charge-separated, polar ground state, which is stabilised with an increase in solvent polarity.[21] In concentration-dependent absorption studies of **BrTPA-Py** (5–50 μM) in DMSO and THF, all the absorbance bands are sharpened and an increase in the absorption intensity is observed (Fig. 2b and c). These studies support the tendency of **BrTPA-Py** molecules to undergo aggregation.[22] Further, compound **BrTPA-Py** is found to be weakly emissive in all organic solvents, such as THF, DMSO and EtOH (Fig. S1, ESI†). Powder X-ray diffraction (PXRD) analysis of a pristine sample of **BrTPA-Py** supports its low crystallinity and reveals the presence of characteristic peaks at 20.76° (d = 4.27 Å), 23.08° (d = 3.85 Å), and 24.11° (d = 3.69 Å), attributed to bromine-related interactions, such as Br···Br (Fig. 3a).[23] Additionally, peaks corresponding to intermolecular π–π stacking and weaker van der Waals interactions are also observed in the PXRD spectrum (Table S3, ESI†). Upon grinding the sample, a single prominent peak around 21° (d = 4.166 Å), attributed to Br···Br interactions is observed in the PXRD spectrum, signifying a transition from a relatively ordered crystalline phase to a disordered/amorphous state, with disturbed packing over a long range.

Encouraged by the favourable photophysical behaviour of the **BrTPA-Py** building block in the solvated state, we examined the self-assembly behaviour of compound **BrTPA-Py** in mixed aqueous media in the presence of DMSO and THF as co-solvents using absorption spectroscopic techniques. The UV-vis spectrum of **BrTPA-Py** in DMSO exhibits strong absorption bands at 301 and 368 nm, corresponding to the π–π* and n–π* transitions of the quinoxaline moiety, respectively, and a broad absorption band at 568 nm (Fig. 3b).[17,24] The addition of water fractions up to 99%, results in the red-shift and broadening of absorption bands at shorter wavelengths (303, 385 nm) as well as longer wavelength (606 nm). This red-shift and broadening of the absorption bands of **BrTPA-Py** in an H_2O : DMSO (99 : 1) solvent mixture indicates at the formation of J-aggregates. We believe that the synergistic effect of Coulombic interactions between dipoles in the D–A–D system and noncovalent interactions between peripheral bromine atoms stabilized the head-to-tail stacking to produce J-aggregates. Absorption studies of **BrTPA-Py** in an H_2O : THF (99 : 1) solvent mixture also exhibit almost similar patterns (Fig. 3c), further confirming the potential of **BrTPA-Py** to generate red-light-absorbing J-type nanoassemblies in mixed aqueous media, irrespective of the kind of co-solvent. In emission studies, solutions of **BrTPA-Py** in H_2O : DMSO as well as H_2O : THF are found to be weakly emissive and, thus, time-resolved fluorescence studies could not be performed to determine radiative/nonradiative constants (Fig. S2, ESI†).

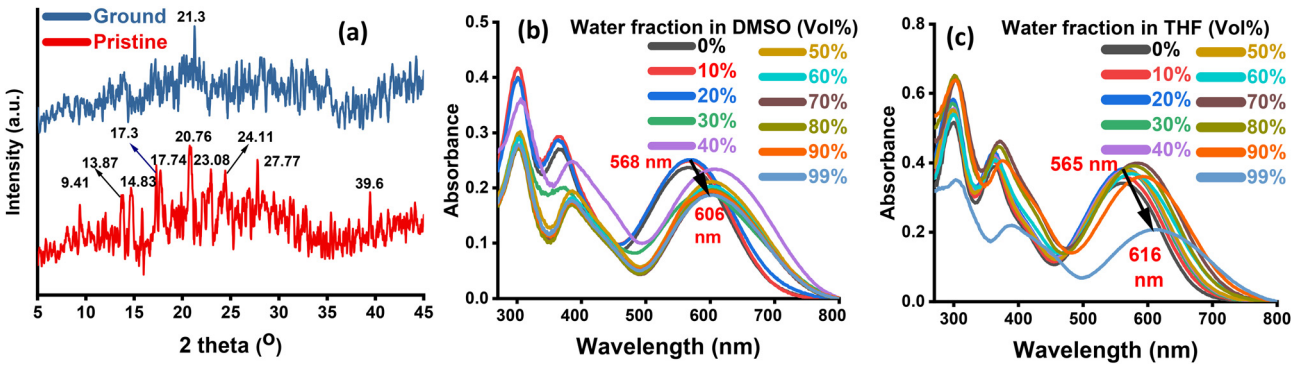

Fig. 3 (a) PXRD spectra of pristine and ground solid of compound **BrTPA-Py**. The UV-vis spectra of **BrTPA-Py** (10 μM) in (b) DMSO and (c) in THF with increasing water fraction.

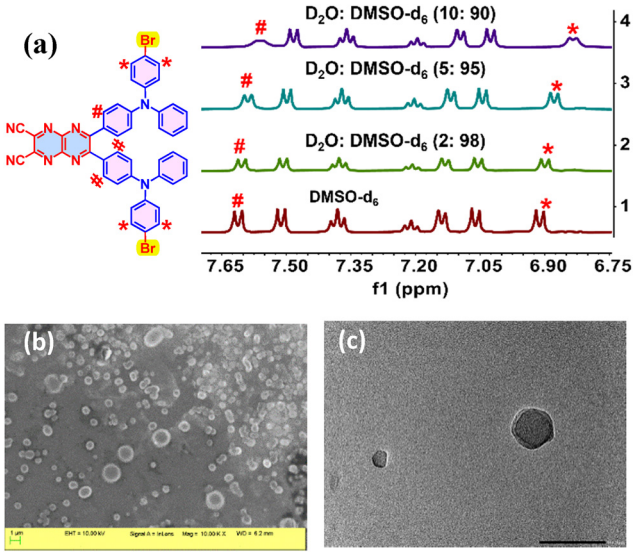

Fig. 4 (a) ^{1}H NMR studies of **BrTPA-Py** in D_2O : DMSO-d_6 solvent mixture. (b) SEM and (c) HRTEM images of **BrTPA-Py** nanoassemblies in H_2O : DMSO (99 : 1) solution, scale bars: 1 μm for the SEM image and 100 nm for the HRTEM image.

To investigate the self-assembly process of **BrTPA-Py** in mixed aqueous solution, ^{1}H NMR studies were conducted using a DMSO-d_6 : D_2O solution (Fig. 4a). Upon the incremental addition of D_2O (up to 10–25 μL) to a 500 μL DMSO-d_6 solution of **BrTPA-Py**, an upfield shift in the aromatic protons is observed, suggesting the significant contribution of intermolecular π–π stacking interactions to the self-assembly behaviour. With a further increase in the proportion of D_2O (25 μL), the aromatic protons in the vicinity of pyrazine nitrogen (at 7.61 ppm, marked as #) and bromine atoms (at 6.91 ppm, marked as *) exhibit a pronounced broadening and a notable decrease in signal intensity. This broadening and eventual suppression of the signals indicate the involvement of a dynamic exchange process in the molecular and aggregated state of **BrTPA-Py**.[25] Thus, orientation-dependent noncovalent interactions, including halogen bonding and π–π stacking, synergistically introduce motional constraints and drive the aggregation process within **BrTPA-Py** assemblies.

Scanning electron microscopy (SEM) and high-resolution transmission electron microscopy (HRTEM) images of **BrTPA-Py** in H_2O : DMSO (99 : 1) solution show the presence of dispersed vesicles of variable size (Fig. 4b and c). In dynamic light scattering (DLS) studies, the average size of **BrTPA-Py** assemblies in H_2O : DMSO (99 : 1) solvent mixture was found to be 106.0 nm (Fig. S3, ESI†).

Cyclic voltammetry (CV) analysis of compound **BrTPA-Py** in dichloromethane (DCM) shows its irreversible oxidation potential (E^1_{ox} = +1.27 V, E^2_{ox} = +1.97 V) and reversible reduction potential (E_{red} = −0.42 V) (Fig. 5a). The excited-state oxidation (E^{1*}_{ox} = −0.41, E^{2*}_{ox} = + 0.29 V) and reduction potential (E^*_{red} = +1.26 V) were determined with the Rehm–Weller equation.[26] The HOMO and LUMO energy levels of **BrTPA-Py** in DCM solution were determined to be −6.02 and −4.34 eV.[26,27]

The optical energy gap (E_g) between the first singlet excited state and the ground state for a DCM solution of **BrTPA-Py** was found to be 1.68 eV, as determined from the Tauc plot (Fig. S4, ESI†). In comparison to the already-reported compound **TPA-Br**, the energy gap was found to be low and the LUMO level was found to be more stabilised, which is attributed to the presence of a strong acceptor in **BrTPA-Py** (Fig. 5b). Electrochemical studies also support the potential of **BrTPA-Py** to activate aerial oxygen ($EO_2/O_2^{\bullet-}$ = −0.33 V) *via* a reductive quenching mechanism.[28] We also performed electrochemical impedance spectroscopy (EIS) studies to examine the charge-transfer process (Fig. 5c). The appearance of a semicircle in the Nyquist plot supports the electrical conductivity of **BrTPA-Py**, which is attributed to its charge-separation characteristics.[29,30]

Encouraged by these studies, we examined the electron transportation potential of **BrTPA-Py** by selecting a three-component system consisting of triethanolamine (TEOA) as a sacrificial donor, and methyl viologen (MV^{2+}) as an acceptor in mixed aqueous media. **BrTPA-Py** in its solvated state

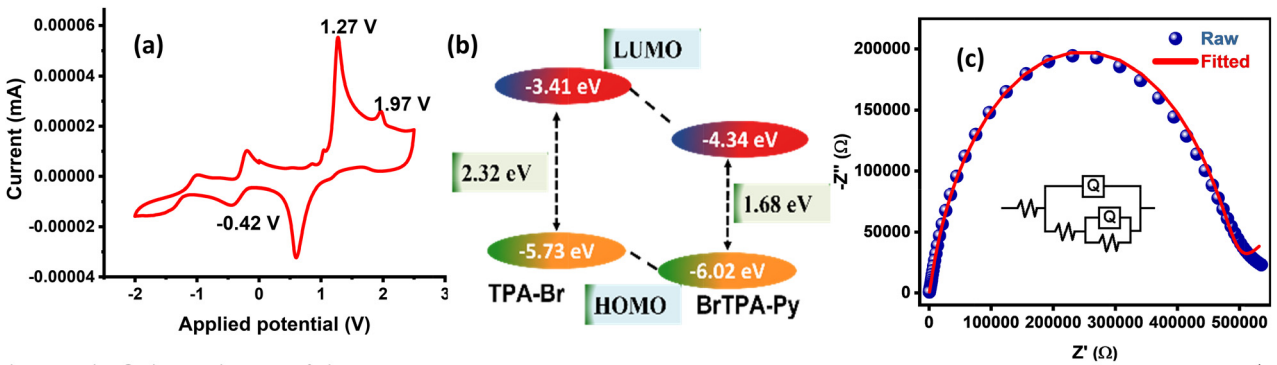

Fig. 5 (a) Cyclic voltammogram of **BrTPA-Py** in dry DCM with 0.1 M tetrabutylammonium hexafluorophosphate (TBAHPF) and potentials measured *vs.* an Ag/AgCl reference electrode. (b) Schematic illustration of the impact of acceptor strength on the energy gap and HOMO–LUMO levels of **BrTPA-Py** and **TPA-Br**. (c) Electrochemical impedance spectroscopic analysis of **BrTPA-Py** using a Nyquist plot.

(DMSO/THF) exhibits no potential for electron transportation upon red-light irradiation. Interestingly, it took only 5 min for **BrTPA-Py** nanoassemblies to transport electrons from donor to acceptor units in an H_2O : DMSO (99 : 1) solvent mixture (Fig. S5a, ESI†). Whereas in an H_2O : THF (99 : 1) solvent mixture, the whole process was complete in a slightly longer time (12 min) (Fig. S5b, ESI†).

Afterwards, we examined the potential of **BrTPA-Py** to activate molecular oxygen for ROS generation under red-light irradiation. The *in situ* generation of singlet oxygen was monitored using 9,10-anthracenediyl-bis(methylene)dimalonic acid (ABDA) as the indicator using two 10 W red LEDs as the source of irradiation.[7,15] Compound **BrTPA-Py** does not show any potential to generate singlet oxygen in a solvated state under red-light irradiation, which is attributed to low absorption by the building block in the long-wavelength region (Fig. S6a and b, ESI†). In an H_2O : DMSO (99 : 1) solvent mixture, a 54.85% decrease in the absorption intensity of ABDA was observed and the rate of decomposition of ABDA (k_{ABDA}) was found to be 10.772×10^{-2} min^{-1} under red-LED irradiation (Fig. 6a and S6c, ESI†). Interestingly, the small amount (1%) of co-solvent (THF/DMSO) had a significant impact on the photosensitization potential of **BrTPA-Py** nanoassemblies in aqueous media. Upon switching the co-solvent (DMSO) in H_2O : THF (99 : 1) solution, the absorption intensity of ABDA was quenched to 36.7% and the value of k_{ABDA} was found to be 5.494×10^{-2} min^{-1} under red-light irradiation (Fig. S7a and b, ESI†). The high singlet oxygen generation capability of **BrTPA-Py** in an H_2O : DMSO (99 : 1) solvent mixture is attributed to the high polarity of the solution, which stabilises the charge-separated state of the nanoassemblies, so that ISC is enhanced and activation of molecular oxygen is boosted. The generation of singlet oxygen by **BrTPA-Py** nanoassemblies in H_2O : DMSO (99 : 1) solution under red-light irradiation was further confirmed by electron paramagnetic resonance (EPR) measurements using 2,2,6,6-tetramethylpiperidine (TEMP) as a spin trap (Fig. S7c, ESI†). As a reference, we also examined the potential of rose bengal (**RB**) to generate singlet oxygen under red-light irradiation, when 7.55% quenching of ABDA absorption intensity was observed and the k_{ABDA} value was found to be 0.441×10^{-2} min^{-1} (Fig. 6b and S7d, ESI†). This is attributed to poor absorption of **RB** under red-light irradiation. We also examined the potential of **BrTPA-Py** nanoassemblies to generate singlet oxygen under white-LED irradiation. The absorption band intensity of ABDA significantly decreased (76%) in H_2O : DMSO (99 : 1) under 50 W white-LED irradiation (Fig. 6c). Although **BrTPA-Py** assemblies exhibited relatively high potential to generate singlet oxygen upon exposure to visible light, their photosensitization activity under red-light as the source of energy is advantageous due to its lower energy consumption.

Next, we investigated the ability of **BrTPA-Py** nanoassemblies (10 μM) to generate superoxide radical anions in various solvents, such as DMSO, THF, H_2O : DMSO (99 : 1) and H_2O : THF (99 : 1) solvent mixture using *N*,*N*,*N*′,*N*′-tetramethyl-*p*-phenylenediamine (TMPD, 100 μM) as an indicator, following standard procedures.[7,15] Compound **BrTPA-Py** did not exhibit any potential to generate superoxide radical anions in the solvated state (DMSO/THF solutions) while **BrTPA-Py** nanoassemblies exhibited relatively high potential to generate superoxide radical anions in H_2O : DMSO (99 : 1) solution in comparison to that in an H_2O : THF (99 : 1) solvent mixture (after 4 min) under irradiation with red-light (Fig. 7a). The generation of superoxide radical anions by **BrTPA-Py** nanoassemblies in H_2O : DMSO (99 : 1) solution under red-light irradiation was further monitored by employing dihydroethidium (DHE) as an indicator using emission spectroscopy. The emission studies showed superoxide radical anion induced enhancement in the emission of DHE in an irradiated solution of **BrTPA-Py** nanoassemblies in H_2O : DMSO (99 : 1), confirming the type I photosensitizing activity of **BrTPA-Py** nanoassemblies (Fig. S8a, ESI†).[31,32] We also examined the potential of the type I reference crystal violet to generate superoxide radical anions under a similar set of experimental conditions[33] and the outcome was comparable with that of **BrTPA-Py** nanoassemblies (Fig. 7b). All these studies support the potential of **BrTPA-Py** nanoassemblies to exhibit type I and type II photosensitizing activity upon irradiation with red-light, which is better/comparable to their respective references. Although **TPA-Br** nanoassemblies exhibit high photosensitization potential under white-LED irradiation,[15] due to their insignificant potential to

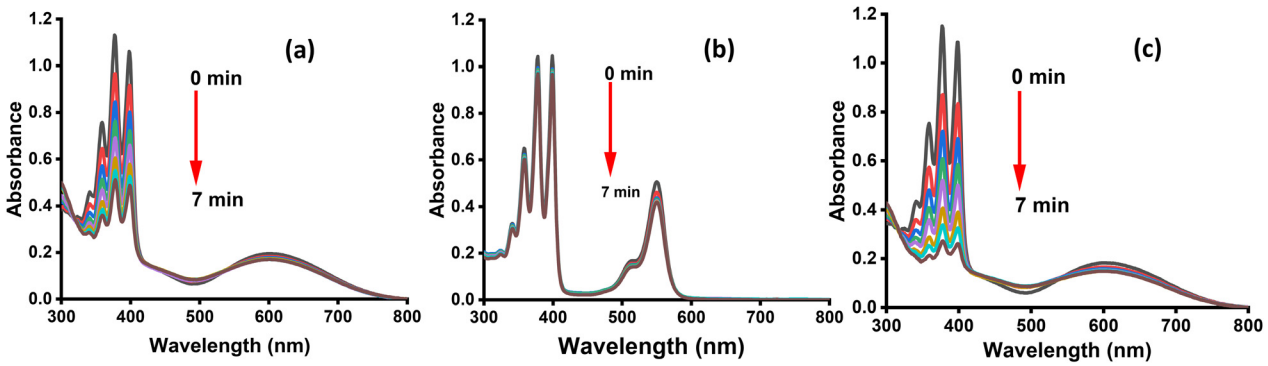

Fig. 6 UV-vis spectra of ABDA (100 μM) in the presence of **BrTPA-Py** (10 μM) in (a) H_2O : DMSO (99 : 1) under irradiation by two 10 W red LEDs and (c) in H_2O : DMSO (99 : 1) under 50 W white LED and aerial oxygen. (b) UV-vis spectra of ABDA (100 μM) in the presence of RB (10 μM) in H_2O : DMSO (99 : 1) solvent mixture under irradiation by two 10 W red LEDs and aerial oxygen.

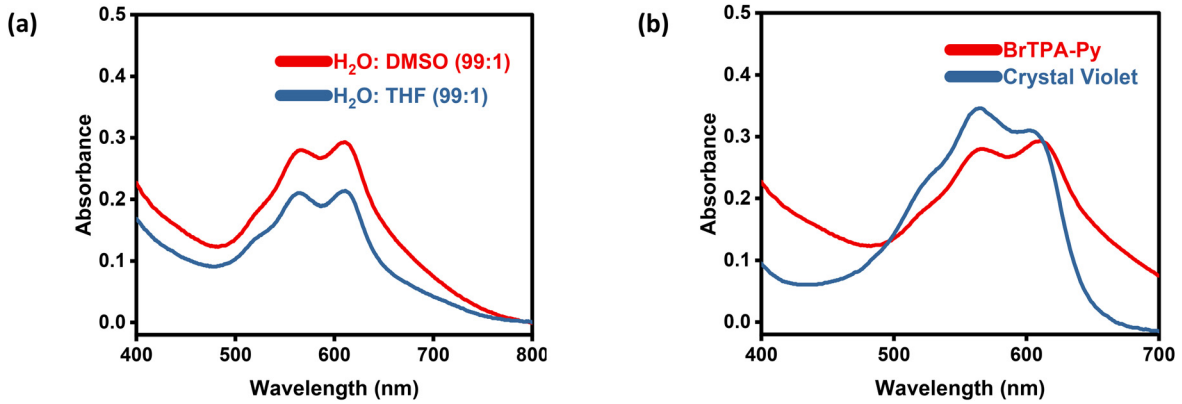

Fig. 7 UV-vis absorption spectra showing the comparative generation of cationic radical species of TMPD (100 μM) in the presence of (a) **BrTPA-Py** (10 μM) in H_2O : DMSO (99 : 1) and H_2O : THF (99 : 1) solvent mixtures, and (b) **BrTPA-Py** and crystal violet in H_2O : DMSO (99 : 1) solution after 4 min exposure to irradiation from two 10 W red LEDs under aerial oxygen.

absorb in the red-light region, the generation of singlet oxygen (13.94% quenching of ABDA, $k_{ABDA} = 1.115 \times 10^{-2}$ min^{-1}) and superoxide radical anions was found to be very low (Fig. 8a and b and S8b, ESI†).

Based on literature reports and experimental studies, we propose that the enhanced ROS generation and oxidative photocatalytic activity of red-light-absorbing **BrTPA-Py** nanoassemblies under low-energy irradiation arise from multiple synergistic factors, including strong charge-transfer characteristics, the incorporation of heavy atoms, and supramolecular aggregation induced by water. In the dispersed state, **BrTPA-Py** is non-emissive and shows no ability to activate aerial oxygen, which we attribute to the dominance of nonradiative decay resulting from its strong charge-transfer characteristics. Upon adding water to DMSO (99%), highly charge-separated supramolecular **BrTPA-Py** nanoassemblies are produced. Although these nanoassemblies remain weakly emissive due to the presence of the charge-separated state, they exhibit significantly enhanced type I and type II ROS generation potential compared to the dispersed phase. This enhancement is attributed to the combined effect of restricted nonradiative decay (*via* halogen···halogen noncovalent interactions)/radiative

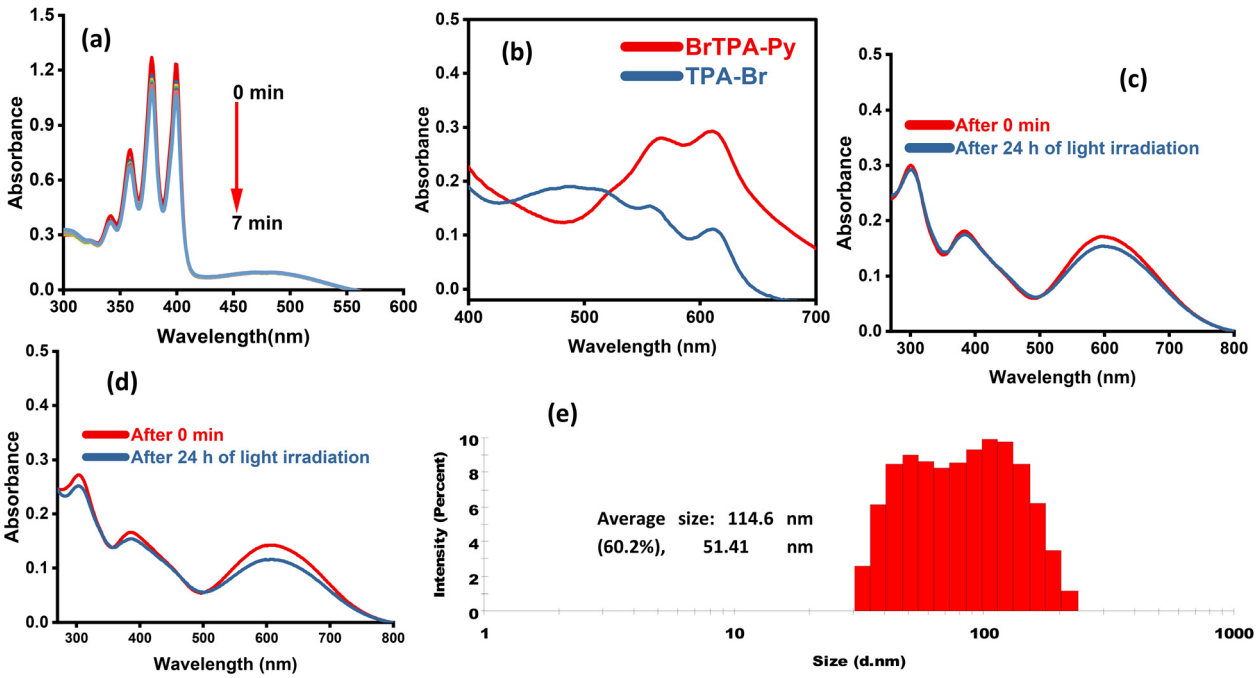

Fig. 8 (a) UV-vis spectra of ABDA (100 μM) in the presence of **TPA-Br** nanoassemblies (10 μM) in H_2O : DMSO (99 : 1) solvent mixture under irradiation by two 10 W red LEDs and air. (b) UV-vis absorption spectra showing the comparative generation of cationic radical species of TMPD (100 μM) in the presence of **BrTPA-Py** and **TPA-Br** in H_2O : DMSO (99 : 1), after 4 min exposure to irradiation from two 10 W red LEDs and aerial oxygen. UV-vis absorption spectra **BrTPA-Py** in (c) H_2O : DMSO (99 : 1) and (d) H_2O : THF (99 : 1) solution after 24 h irradiation under irradiation from two 10 W red LEDs. (e) DLS studies of **BrTPA-Py** in H_2O : DMSO (99 : 1) solution after 24 h irradiation under irradiation from two 10 W red LEDs.

Table 1 Optimisation of reaction conditions for oxidation of triphenylphosphine[a]

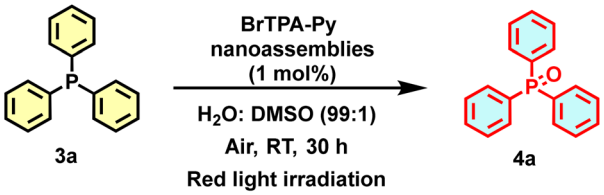

S.N.	Solvent	Catalyst (mol%)	Time	Yield[a] (%)
1	H_2O : DMSO (99 : 1)	**BrTPA-Py** (1)	30 h	92
2[b]	H_2O : DMSO (99 : 1)	**BrTPA-Py** (1)	30 h	N.R.
3	DMSO	**BrTPA-Py** (1)	30 h	N.R.
4	THF	**BrTPA-Py** (1)	30 h	N.R.
5	H_2O : THF (99 : 1)	**BrTPA-Py** (1)	30 h	70
6[c]	H_2O : DMSO (99 : 1)	**BrTPA-Py** (1)	22 h	95
7	H_2O : DMSO (99 : 1)	**TPA-Br** (1)	30 h	N.R.
8	H_2O : DMSO (99 : 1)	—	30 h	N.R.
9[d]	H_2O : DMSO (99 : 1)	**BrTPA-Py** (1)	30 h	N.R.
10[e]	H_2O : DMSO (99 : 1)	**BrTPA-Py** (1)	30 h	N.R.
11	H_2O : DMSO (99 : 1)	**BrTPA-Py** (1)	15 h	43
12	H_2O : DMSO (99 : 1)	**BrTPA-Py** (0.5)	30 h	60
13	H_2O : DMSO (99 : 1)	**BrTPA-Py** (2)	24 h	96

[a] Reaction conditions: **3a** (100 mg, 0.38 mmol), **BrTPA-Py** nanoassemblies (1 mol%), 10 mL of H_2O : DMSO (99 : 1) solvent mixture, 30 h, under air, two 10 W red LEDs. Isolated yield. [b] Without light irradiation at 50 °C. N.R. = no reaction. RT = room temperature. [c] Under 50 W white-LED irradiation. [d] Under inert atmosphere. [e] Without light irradiation.

decay (due to strong charge-transfer characteristics) and heavy-atom-induced SOC, which facilitated ISC by minimizing energy loss and enabled the effective activation of molecular oxygen through both electron transfer (type I) and energy transfer (type II) mechanisms.

Given the excellent photosensitization potential of **BrTPA-Py** nanoassemblies to generate ROS in an H_2O : DMSO (99 : 1) solvent mixture, we planned to explore their photocatalytic potential in oxidative organic transformations under red-light radiation. We chose the oxidation of triaryl phosphines as a test reaction. Before setting up the reactions, we evaluated the photostability of **BrTPA-Py** nanoassemblies in the H_2O : DMSO (99 : 1) and H_2O : THF (99 : 1) solvent systems by continuously exposing the solution to red-light for 24 hours. The absorbance of **BrTPA-Py** nanoassemblies decreased to 10% in H_2O : DMSO (99 : 1) and 18.31% in H_2O : THF (99 : 1) (Fig. 8c and d), indicating their strong photostability. Additionally, DLS analysis showed negligible variation in the size of the **BrTPA-Py** nanoassemblies in H_2O : DMSO (99 : 1) solution even after 24 hours of exposure to red LED light, strongly confirming their photostability (Fig. 8e).

Encouraged by the outcome of the above studies, we set up the oxidative transformation of triarylphosphine as a model reaction in H_2O : DMSO (99 : 1) solution using 1.0 mol% of **BrTPA-Py** nanoassemblies as a catalyst under red-light irradiation (Table 1). The reaction progressed smoothly to furnish the desired product (**4a**) within 30 h. Although several photocatalysts have been developed to catalyse the oxidation of phosphines,[8,34] to date, there has been no report regarding photocatalytic activity under low-energy radiation (Fig. 9a and Table S1†). Amazingly, **BrTPA-Py** nanoassemblies efficiently catalyse the test reaction to furnish the target product, triphenylphosphine oxide (**4a**), in 92% yield (after purification) under mild reaction conditions (Fig. 9b and Table 1, entry 1). We also conducted the reaction under thermal conditions (50 °C) in the absence of any irradiation,

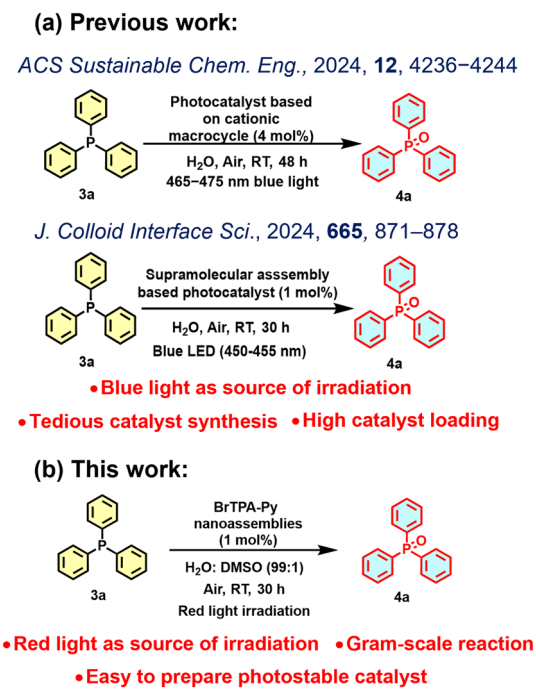

Fig. 9 Comparison of (a) recent literature reports of the photocatalyzed oxidation of triarylphosphine in water with (b) the present work.

but the formation of the target product (**4a**) was not detected. This study confirms that the reaction is not catalysed by heat generated during photoirradiation (Table 1, entry 2). Afterwards, we examined the impact of the solvent on the oxidation reaction. The test reaction did not yield any desired product in DMSO or THF, while the target product (**4a**) was obtained in relatively lower yield (70%) in H_2O : THF (99 : 1) (Table 1, entries 3–5). We also examined the effect of visible-light irradiation (50 W white LED) on the reaction. Under white-LED light after 22 h, the target product (**4a**) was obtained in 95% yield (Table 1, entry 6). The comparable yield along with the energetic advantages of red-light irradiation point to the success of the design strategy. As a test, we also examined the catalytic potential of **TPA-Br** nanoassemblies under red-LED irradiation but the formation of the target product (**4a**) was not detected (Table 1, entry 7). The formation of the target product (**4a**) was also not observed under the optimised conditions in the absence of light irradiation, catalyst or aerial oxygen (Table 1, entries 8–10). Additionally, when the reaction time was reduced to 15 h, the yield of the target product (**4a**) dropped significantly (43%) (Table 1, entry 11). These studies confirm that all three components, *i.e.*, light irradiation, aerial atmosphere and **BrTPA-Py** nanoassemblies, are vital for completion of the oxidation of triphenyl phosphine under red-light irradiation. Next, the effect of catalyst loading on reaction yield was examined. Upon decreasing the catalyst loading of **BrTPA-Py** nanoassemblies to 0.5 mol%, the reaction yields decreased and the target product (**4a**) was obtained in 60% yield (Table 1, entry 12). Whereas, upon increasing the loading of **BrTPA-Py** nanoassemblies to 2 mol%, complete conversion within 24 h was observed with slightly improved yield (96%) (Table 1, entry 13). Considering the small increase in the yield, on balance, we chose 1 mol% as the optimum catalyst loading for further study.

After optimizing the reaction conditions for aerobic photooxidation, the substrate scope of **BrTPA-Py** nanoassemblies as photocatalyst was determined in the oxidation of triarylphosphines (**3**) (Scheme 2). The **BrTPA-Py** nanoassemblies catalysed the aerobic photooxidation of electron-rich phosphines (tri(*p*-methoxy)phosphine (**3b**) and tri(*p*-methyl)phosphine (**3c**)) to produce the corresponding products (**4b**, **4c**) in excellent yields. Conversely, the presence of an electron-withdrawing group (–F, **3d**) at the *para* position and the presence of steric hinderance in tris(2-methylphenyl)phosphine (**3e**) significantly altered the progress of the reaction, and the target products (**4d** and **4e**) were obtained in 55 and 73% yields, respectively.

To examine the scale-up possibility of using **BrTPA-Py** nanoassemblies as the catalyst, we set up the preparation of triphenylphosphine oxide (**4a**) under optimised conditions (Scheme 3). The reaction yielded the desired product (**4a**) in 58% yield in 40 h, demonstrating the scale-up catalytic potential of **BrTPA-Py** nanoassemblies.

To understand the mechanism, we performed several controlled experiments by setting up the model reaction using triphenyl phosphine (**3a**) as the model substrate (Fig. 10a). The

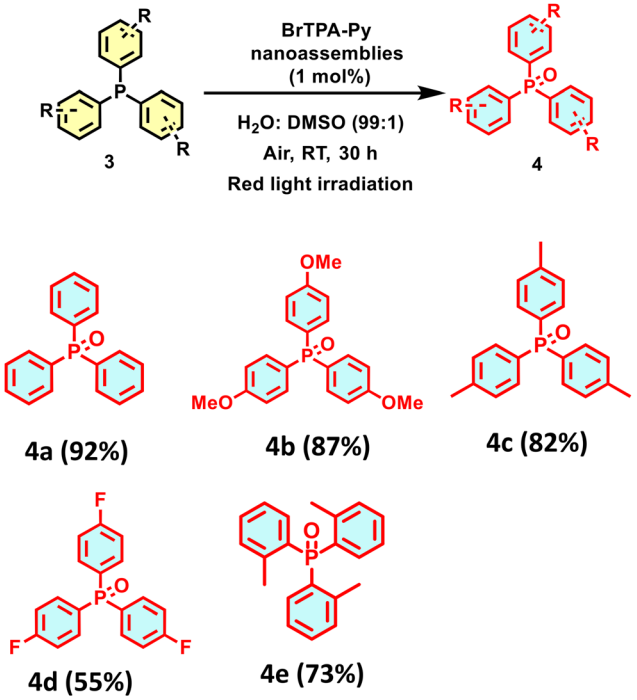

Scheme 2 Substrate scope of **BrTPA-Py** nanoassemblies catalysed photooxidation of triaryl phosphines. Reaction conditions: **3** (100 mg, 1 equiv.), **BrTPA-Py** nanoassemblies (1 mol%), 10 mL of H_2O : DMSO (99 : 1) solvent mixture, 30 h, under air, two 10 W red LEDs. Isolated yield.

reaction was repeated in the presence of a radical scavenger 2,2,6,6-tetramethylpiperidine-*N*-oxyl (TEMPO) under the optimised conditions and the desired product (**4a**) was obtained in 27% yield, suggesting the participation of a radical intermediate in the mechanistic pathway. Upon the addition of singlet oxygen scavengers (NaN_3 and DABCO), the yield of the final product (**4a**) was reduced to 16% and 11%, respectively, whereas in the presence of a type I ROS scavenger (*p*-benzoquinone, *p*-BQ), the reaction yield was not much affected. These studies confirm that the reaction progress is facilitated by singlet oxygen.

Based upon the outcome of all the control experiments and literature reports,[8,34–36] a plausible mechanism is proposed (Fig. 10b). Photoexcited **BrTPA-Py** nanoassemblies (PS) under red-light irradiation activate aerial oxygen ($^3O_2$) through an energy transfer pathway to generate singlet oxygen ($^1O_2$).

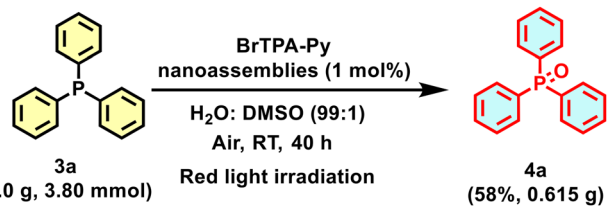

Scheme 3 The gram-scale synthesis of triphenylphosphine oxide using **BrTPA-Py** nanoassemblies. Reaction conditions: **3a** (1 g, 3.8 mmol), **BrTPA-Py** nanoassemblies (1 mol%), 30 mL of H_2O : DMSO (99 : 1) solvent mixture, 40 h, under air, two 10 W red LEDs. Isolated yield.

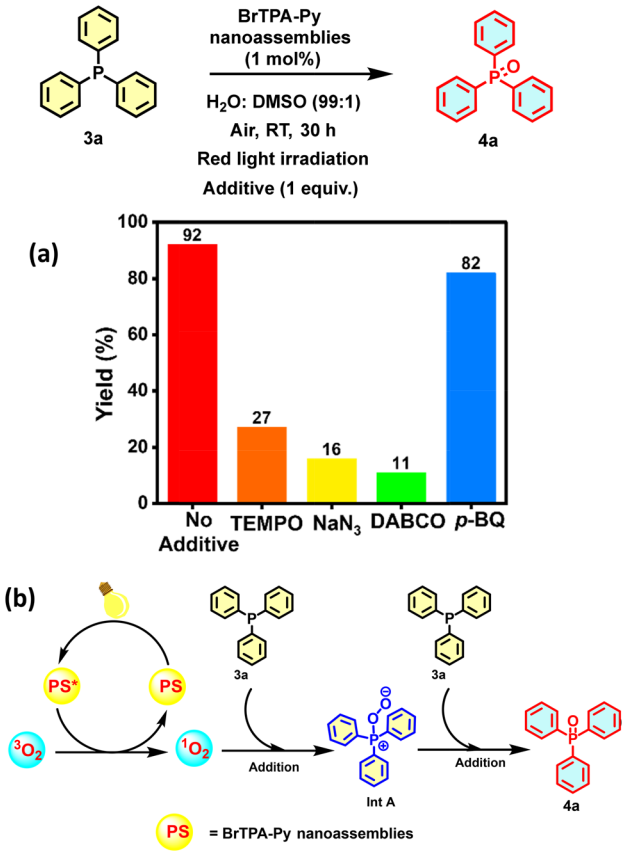

Fig. 10 (a) Controlled experiments in **BrTPA-Py** nanoassemblies catalysed photooxidation of triaryl phosphine under optimized reaction conditions in the presence of various quenching agents (1 equiv.). (b) The proposed mechanism for **BrTPA-Py** nanoassemblies catalysed photooxidation of triarylphosphine under aerial oxygen.

Afterwards, reductive triphenylphosphine (**3a**) and oxidative singlet oxygen underwent single-electron oxidation to afford intermediate **A**, which upon reaction with a second molecule of phosphine (**3a**), furnished the final product (**4a**).

To understand the potential of **BrTPA-Py** nanoassemblies to catalyse the oxidative transformation through an electron transfer pathway (with the superoxide radical anion as oxidant), we evaluated the catalytic efficiency of **BrTPA-Py** nanoassemblies in the oxidative hydrolysis of boronic acids. We set up the model reaction using 4-cyanophenylboronic acid (**5a**) as the substrate and *N*,*N*-diisopropylethylamine (DIPEA) as the base (10 equiv.) in H_2O : DMSO (99 : 1) solution (Table 2).

The model reaction proceeded well under red-LED light irradiation to furnish the target product (**6a**) in 94% yield in 12 h (Table 2, entry 1). The reaction took 42 h to furnish the desired product in 85% yield when the proportion of DIPEA was reduced (5 equiv. of DIPEA) (Table 2, entry 2). Upon switching the base strength (triethylamine (TEA)/1,8-diazabicyclo(5.4.0)undec-7-ene (DBU)), the product (**6a**) was obtained in lower yield (Table 2, entries 3, 4). All these studies highlight the important contribution of a sacrificial donor for switching the energy transfer pathway to an electron transfer pathway. The yield of target product (**6a**) was also affected by changing the co-solvent (Table 2, entry 5). Further, the formation of the desired product was not observed in the absence of catalyst/base/red-light irradiation/aerial oxygen, signifying the strong influence of all of them on the progress of the reaction to completion (Table 2, entries 6–9). The impact of catalyst amount on the reaction rate was observed upon reducing/increasing the catalyst

Table 2 Optimisation of reaction conditions for the oxidative hydroxylation of arylboronic acids[a]

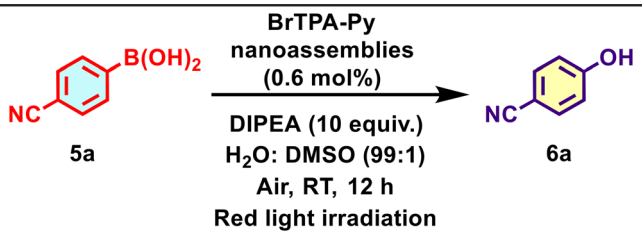

S.N.	Solvent	Catalyst (mol%)	Base	Time	Yield (%)
1	H_2O : DMSO (99 : 1)	**BrTPA-Py** (0.6)	DIPEA (10 equiv.)	12 h	94
2	H_2O : DMSO (99 : 1)	**BrTPA-Py** (0.6)	DIPEA (5 equiv.)	42 h	85
3	H_2O : DMSO (99 : 1)	**BrTPA-Py** (0.6)	TEA (10 equiv.)	12 h	50
4	H_2O : DMSO (99 : 1)	**BrTPA-Py** (0.6)	DBU (10 equiv.)	12 h	39
5	H_2O : THF (99 : 1)	**BrTPA-Py** (0.6)	DIPEA (10 equiv.)	12 h	75
6	H_2O : DMSO (99 : 1)	**BrTPA-Py** (0.6)	—	12 h	N.R
7	H_2O : DMSO (99 : 1)	—	DIPEA (10 equiv.)	12 h	N.R.
8[b]	H_2O : DMSO (99 : 1)	**BrTPA-Py** (0.6)	DIPEA (10 equiv.)	12 h	N.R.
9[c]	H_2O : DMSO (99 : 1)	**BrTPA-Py** (0.6)	DIPEA (10 equiv.)	12 h	N.R.
10	H_2O : DMSO (99 : 1)	**BrTPA-Py** (0.4)	DIPEA (10 equiv.)	12 h	70
11	H_2O : DMSO (99 : 1)	**BrTPA-Py** (1)	DIPEA (10 equiv.)	10 h	97
12	H_2O : DMSO (99 : 1)	**TPA-Br** (0.6)	DIPEA (10 equiv.)	12 h	N.R.

[a] Reaction conditions: **5a** (100 mg, 0.68 mmol), base (10 equiv.), **BrTPA-Py** nanoassemblies (0.6 mol%), 10 mL of H_2O : DMSO (99 : 1) solvent mixture, 12 h, under air, two 10 W red LEDs. Isolated yield. [b] Under inert atmosphere, [c] Without light irradiation. RT = room temperature. N. R. = no reaction.

loading (0.4 mol%/1 mol%), and 0.6 mol% of **BrTPA-Py** nanoassemblies was chosen as the optimum catalyst loading (Table 2, entries 10, 11). As a test, we also examined the progress of the model reaction using **TPA-Br** nanoassemblies as the catalyst under optimised reaction conditions, but the formation of the target product (**6a**) was not detected, confirming the dependence of the progress of the reaction upon absorption by the photocatalyst in the red-light region (Table 2, entry 12).

To verify the universality of **BrTPA-Py** nanoassemblies as photocatalyst for oxidative hydroxylation, we examined a variety of substituted substrates under the optimised reaction conditions (Scheme 4). For reaction substrates with electron-withdrawing groups (EWG), such as –CN, $–NO_2$, –F, –Cl, –CHO, or $–C(=O)CH_3$, the desired products (Scheme 4, **6a–6f**) were obtained in high yields. Conversely, the test reactions of arylboronic acid with electron-donating groups under optimised conditions furnished the desired products (Scheme 4, **6g–6h** in relatively lower yield.

To get further insight into the reaction mechanism, we carried out several control experiments by selecting the **BrTPA-Py** nanoassemblies catalysed oxidative hydroxylation of 4-cyanophenylboronic acid (**5a**) as the model reaction (Fig. S9, ESI†). The presence of a radical scavenger (TEMPO) as well as a singlet oxygen quencher (NaN_3/DABCO) in the test reaction had an insignificant influence on the outcome of the reaction, overriding the participation of radical intermediates or singlet oxygen in the progress of the reaction. Conversely, the progress of the reaction was found to be strongly inhibited in the presence of *p*-BQ as a superoxide radical anion scavenger. On the basis of these experiments and literature reports,[7] we believe that **BrTPA-Py** nanoassemblies (PS) after photoexcitation generate radical anion species ($PS^{\bullet-}$) in the presence of the sacrificial donor DIPEA (Fig. 11). The photoexcited radical anion further activates molecular oxygen to produce a superoxide radical anion ($O_2^{\bullet-}$), which in turn activates arylboronic acid (**5a**) to furnish the desired product (**6a**) through the participation of intermediates **I–III**.

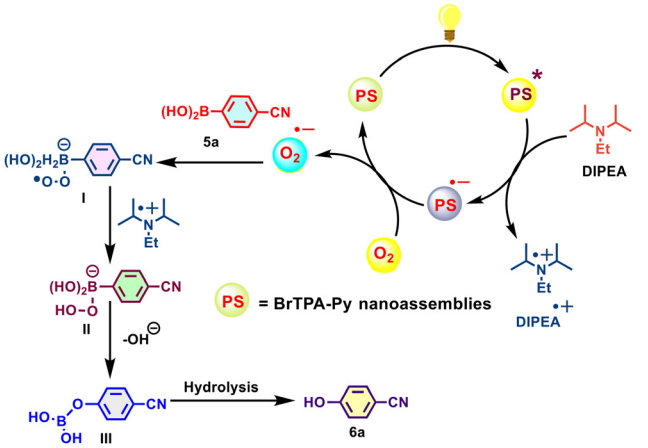

Fig. 11 Proposed mechanism for **BrTPA-Py** nanoassemblies catalysed photooxidative hydroxylation of arylboronic acids.

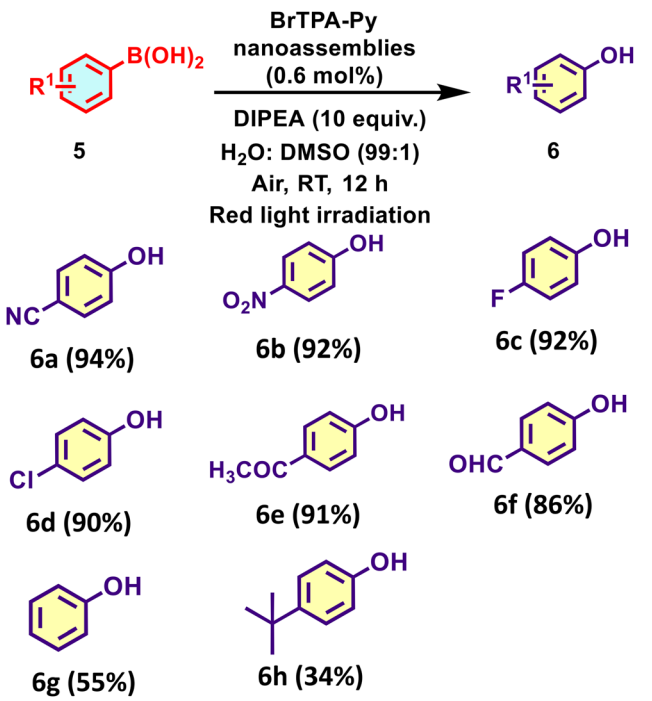

Scheme 4 Substrate scope of **BrTPA-Py** nanoassemblies photocatalysed oxidative hydroxylation of arylboronic acids. Reaction conditions: **5** (100 mg, 1 equiv.), DIPEA (10 equiv.), **BrTPA-Py** nanoassemblies (0.6 mol%), 10 mL of H_2O : DMSO (99 : 1) solvent mixture, 12 h, under air, two 10 W red LEDs. Isolated yield.

Conclusions

We have developed red-light-absorbing supramolecular assemblies in aqueous media using the D–A–D building block **BrTPA-Py**. By endowing the **BrTPA-Py** nanoassemblies with strong charge-transfer characteristics and inducing Br···Br interactions through the strategic incorporation of bromine atoms at peripheral positions, radiative/nonradiative energy leakage was blocked with the simultaneous promotion of activation of aerial oxygen through energy/electron transfer pathways. The excellent photosensitizing activity of **BrTPA-Py** nanoassemblies in aqueous media was utilised to catalyse oxidative transformations, including the photooxidation of triarylphosphines (type II) and the oxidative hydroxylation of arylboronic acid (type I), under mild conditions (room temperature, red-light irradiation, and air as the oxidant). The potential of **BrTPA-Py** nanoassemblies to catalyse an oxidative transformation at gram-scale level was also revealed. The work presented in the paper demonstrates a simple strategy to generate red-light-absorbing supramolecular photosensitizing assemblies for efficient, green and sustainable photocatalysis by equipping the building block with strong charge-transfer characteristics, and halogen-induced noncovalent interactions in the assembled state.

Data availability

All data recorded and analysed for the preparation of this manuscript are included in this article and its ESI.† The ESI is available free of charge and includes the following: The general experimental and spectral data, ^{1}H NMR, ^{13}C NMR spectra, and HRMS analysis data of compound **BrTPA-Py**. ^{1}H, ^{13}C and ^{31}P NMR spectrum of compound **4a** and ^{1}H NMR, ^{13}C NMR spectrum of compounds **4b–4e**, **6a–6h**. DLS, Electron transportation, Singlet oxygen generation (procedure for singlet oxygen generation, Graphs for decomposition rate constant of ABDA), table of comparison of present manuscript with previous literature reports and characterisation data of compounds **4a–4e**, **6a–6h** (PDF).

Author contributions

A. S. contributed to conceptualization, methodology, data recording, data analysis and writing of the original draft. M. K. contributed to conceptualization, methodology, writing – reviewing and editing. V. B. contributed to project administration, supervision, conceptualization, methodology, data analysis, writing – reviewing and editing. The manuscript was written through contribution of all authors. All authors have given approval to the final version of the manuscript.

Conflicts of interest

There are no conflicts to declare.

Acknowledgements

V. B. is thankful to SERB, New Delhi (ref no. CRG/2022/003279) for financial support. A. S. is thankful to CSIR, New Delhi for Senior Research Fellowship (SRF).

References

1 A. H. Schade and L. Mei, *Org. Biomol. Chem.*, 2023, **21**, 2472–2485.
2 P. Yan, R. Zeng, B. Bao, X. M. Yang, L. Zhu, B. Pan, S. L. Niu, X. W. Qi, Y. L. Li and Q. Ouyang, *Green Chem.*, 2022, **24**, 9263–9268.
3 H. Wei, X. Li, F. Huang, S. Wu, H. Ding, Q. Chen, M. Li and X. Lang, *Chin. Chem. Lett.*, 2023, **34**, 108564.
4 X. Dong, F. Zhang, F. Huang and X. Lang, *Appl. Catal., B*, 2022, **318**, 121875.
5 H. Zhang, T. Yuan, N. Zhumabay, Z. Ruan, H. Qian and M. Rueping, *Chem. Sci.*, 2024, **15**, 17435–17443.
6 K. K. Niu, T. X. Luan, J. Cui, H. Liu, L. B. Xing and P. Z. Li, *ACS Catal.*, 2024, **14**, 2631–2641.
7 S. Yu, R. X. Zhu, K. K. Niu, N. Han, H. Liu and L. B. Xing, *Chem. Sci.*, 2024, **15**, 1870–1878.
8 R. Z. Dong, X. H. Shi, H. Liu, S. Yu, K. K. Niu and L. B. Xing, *J. Colloid Interface Sci.*, 2024, **665**, 871–878.
9 S. Guo, D. Gu, Y. Yang, J. Tian and X. Chen, *J. Nanobiotechnol.*, 2023, **21**, 348.
10 P. Chinna Ayya Swamy, G. Sivaraman, R. N. Priyanka, S. O. Raja, K. Ponnuvel, J. Shanmugpriya and A. Gulyani, *Coord. Chem. Rev.*, 2020, **411**, 213233.
11 S. Dadwal, M. Kumar and V. Bhalla, *J. Org. Chem.*, 2020, **85**, 13906–13919.
12 G. Kaur, H. Kaur, M. Kaur, M. Kumar and V. Bhalla, *Aggregate*, 2022, **3**, e171.
13 M. Singh, M. Kumar and V. Bhalla, *Chem. – Asian J.*, 2024, **19**, e202400033.
14 G. Singh, M. Singh, S. Kumar, M. Kumar and V. Bhalla, *Asian J. Org. Chem.*, 2021, **10**, 2596–2602.
15 A. Singh, M. Kumar and V. Bhalla, *ACS Appl. Mater. Interfaces*, 2024, **16**, 62064–62081.
16 R. Lin, J. Liu, W. Xu, Z. Liu, X. He, C. Zheng, M. Kang, X. Li, Z. Zhang, H.-T. Feng, J. W. Y. Lam, D. Wang, M. Chen and B. Z. Tang, *Adv. Mater.*, 2023, **35**, 2303212.
17 M. Chen, X. Zhang, J. Liu, F. Liu, R. Zhang, P. Wei, H. Feng, M. Tu, A. Qin, J. W. Y. Lam, D. Ding and B. Z. Tang, *ACS Nano*, 2020, **14**, 4265–4275.
18 K. Wen, H. Tan, Q. Peng, H. Chen, H. Ma, L. Wang, A. Peng, Q. Shi, X. Cai and H. Huang, *Adv. Mater.*, 2022, **34**, 2108146.
19 D. Zhao, L. Zhang, M. Yin, Z. He, F. Fang, M. Zhan, S. Tian, F. Meng and L. Luo, *Aggregate*, 2024, **5**, e576.
20 Q. Jiang, J. Li, Z. Du, M. Li, L. Chen, X. Zhang, X. Tang, Y. Shen, D. Ma, W. Li, L. Li, N. Alifu, Q. Hu and J. Liu, *Adv. Healthcare Mater.*, 2024, **13**, 2400962.
21 S. Franzese, N. Saker Neto and W. W. H. Wong, *Chem. – Eur. J.*, 2024, **30**, e202400314.
22 G. Kumar, M. Kumar and V. Bhalla, *ACS Appl. Mater. Interfaces*, 2024, **16**, 62988–62998.
23 M. Capdevila-Cortada and J. J. Novoa, *CrystEngComm*, 2015, **17**, 3354–3365.
24 B. K. Sharma, A. M. Shaikh, S. Chacko and R. M. Kamble, *J. Chem. Sci.*, 2017, **129**, 483–494.
25 S. Lindblad, K. Mehmeti, A. X. Veiga, B. Nekoueishahraki, J. Gräfenstein and M. Erdélyi, *J. Am. Chem. Soc.*, 2018, **140**, 13503–13513.
26 L. Mei, J. M. Veleta and T. L. Gianetti, *J. Am. Chem. Soc.*, 2020, **142**, 12056–12061.
27 S. Sharma and S. Sengupta, *Org. Chem. Front.*, 2023, **10**, 6087–6095.
28 Y. Nosaka and A. Y. Nosaka, *Chem. Rev.*, 2017, **117**, 11302–11336.
29 H. Tariq and F. Azad, *J. Nanomater.*, 2022, 3855582, DOI: 10.1155/2022/3855582.
30 M. Deng, L. Wang, Z. Wen, J. Chakraborty, J. Sun, G. Wang and P. Van Der Voort, *Green Chem.*, 2024, **26**, 3239–3248.
31 D. Chen, Q. Yu, X. Huang, H. Dai, T. Luo, J. Shao, P. Chen, J. Chen, W. Huang and X. Dong, *Small*, 2020, **16**, 2001059.
32 Z. Fan, K.-X. Teng, Y.-Y. Xu, L.-Y. Niu and Q.-Z. Yang, *Angew. Chem., Int. Ed.*, 2025, **64**, e202413595.
33 J. Zhuang, B. Wang, H. Chen, K. Zhang, N. Li, N. Zhao and B. Z. Tang, *ACS Nano*, 2023, **17**, 9110–9125.
34 X. L. Li, K. K. Niu, F. D. Wang, X. Y. Yao, H. Liu, S. Yu and L. B. Xing, *ACS Sustainable Chem. Eng.*, 2024, **12**, 4236–4244.

35 Y. Zhang, C. Ye, S. Li, A. Ding, G. Gu and H. Guo, *RSC Adv.*, 2017, **7**, 13240–13243.
36 Y. Tanabe, K. Nakajima and Y. Nishibayashi, *Chem. – Eur. J.*, 2018, **24**, 18618–18622.